# Conducting Polyaniline Filaments in a Mesoporous Channel Host

Chun-Guey Wu and Thomas Bein*

**Conducting filaments of polyaniline have been prepared in the 3-nanometer-wide hexagonal channel system of the aluminosilicate MCM-41. Adsorption of aniline vapor into the dehydrated host, followed by reaction with peroxydisulfate, leads to encapsulated polyaniline filaments. Spectroscopic data show that the filaments are in the protonated emeraldine salt form, and chromatography indicates chain lengths of several hundred aniline rings. The filaments have significant conductivity while encapsulated in the channels, as measured by microwave absorption at 2.6 gigahertz. This demonstration of conjugated polymers with mobile charge carriers in nanometer channels represents a step toward the design of nanometer electronic devices.**

Efforts to create electronic functions and devices based on molecules instead of bulk semiconductors are inspired by the anticipated enormous increase in computing speed and storage density (*1*, *2*). Previous studies have shown that conjugated systems with appropriate end groups (*3*–*5*) and confined aromatic systems (*6*) can transfer excitations upon photon absorption or after reduction or oxidation. A major challenge is to achieve charge transfer with low fields as in metallic wires and to establish communication with individual, electrically separated nanometer structures or molecules.

We have demonstrated previously the encapsulation of several different conjugated polymers such as polypyrrole and pyrolyzed polyacrylonitrile in the well-defined channels of zeolite molecular sieves (*7*–*10*). The template synthesis of conducting polymers in the much larger, random pores (about 0.1 to 1 μm) of insulating host membranes has also been described (*11*). Networks of poly(3-methylthiophene) dendrites have been grown between electrodes (*12*). We have now achieved the stabilization of conducting polyaniline filaments in the ordered, 3-nm-wide hexagonal channels of the mesoporous aluminosilicate host (*13*, *14*) MCM-41. We were able to demonstrate the ac conductivity of such encapsulated filaments of nanometer dimensions.

A distinctive feature of polyaniline among the conducting polymers is that its conductivity is not only controlled by the degree of chain oxidation but also by the level of protonation in $\{[(-B-NH-B-NH-)_y(-B-N=Q=N-)_{1-y}](HA)_x\}_n$ (*15*, *16*). In the conducting form [emeraldine salt or polyaniline (PANI)], y is close to 0.5, B and Q are $C_6H_4$ rings in the benzenoid and quinoid states, respectively, and HA is a strong acid. The MCM host was synthesized with $C_{16}H_{33}N(CH_3)_3OH$ according to (*13*) with a Si/Al ratio of 18 and was then calcined at 580°C and evacuated at 400°C and $10^{-5}$ torr. Vacuum-distilled aniline was adsorbed into the host from the vapor phase at 40°C for 24 hours (Fig. 1). The aniline-saturated host (AN-MCM; 0.5 g of aniline in 1.0 g of host) was then immersed in an aqueous solution of peroxydisulfate at 0°C for 4 hours (1:1 molar ratio of oxidant versus aniline, 1 g of AN-MCM in 50 ml of 0.2 M HCl), and a drastic color change to dark green was observed (*17*). After a thorough washing with water, the materials were dried under vacuum. A typical polymer loading was 0.28 g per 1.00 g of MCM host.

Electron micrographs of the MCM host before and after polyaniline encapsulation show the characteristic hexagonal channel pattern (unit cell size, 4.0 nm) in both cases (Fig. 2). The similarity of the ring and C–H bending modes between PANI-loaded host (PANI-MCM) and emeraldine salt, seen in their Raman spectra (Fig. 3), show that the encapsulated polymer is in the conducting, protonated state (*18*). In particular, the modes at 1309 and 1364 $cm^{-1}$ are indicative of the protonated quinone radical cation structure. Infrared spectra of PANI-MCM and of extracted polymer from PANI-MCM resemble the ring vibration pattern of bulk emeraldine salt (peaks at 1585, 1497, 1306, 1240, and 1124 $cm^{-1}$) (*19*). The electronic absorption spectrum of PANI-MCM presents major transitions at 4.6, 3.4 (shoulder), and 1.6 eV, typical for the band-gap and polaron transitions of emeraldine salt (*20*). The encapsulated, evacuated polymer shows a single, fairly broad (8 G) electron spin resonance line at $g = 2.0032$, suggesting slightly lower protonation levels than in emeraldine salt (*21*) or dipolar interactions with the MCM channel walls.

The relative chain length of intrachannel polyaniline [versus polystyrene (PS), in *N*-methylpyrrolidinone with 2.5% LiCl] was determined with gel permeation chromatography after decomposition of the host in 5% HF and deprotonation. Polyaniline is stable toward HF under these conditions. A correction factor of ~0.5 is required to estimate absolute molecular weights (*22*). The peak molecular weight of the intrachannel polyaniline (35,000 versus PS; correction makes it equivalent to ~190 polyaniline rings) is consistently shorter than that of bulk material synthesized under comparable conditions (52,000 versus PS; corrected to ~290 rings). This difference suggests that diffusional constraints experienced by the reactants limit the chain growth in the MCM host.

Infrared spectra of the hydroxyl region of MCM-41 before aniline loading show a single peak at 3650 $cm^{-1}$ (in Nujol), attributable to Si–OH, which disappears on contact with aniline. This indicates complete coverage of the intrachannel surface with aniline. The intrachannel polymerization reaction was probed by nitrogen sorption. The isotherm of the PANI-MCM shows a residual pore volume of 0.40 ml per gram of MCM host, compared with 0.64-ml pore volume in the empty host (Fig. 4). If we assume a polymer density of 1.3 $g/cm^3$ (*23*), the loading of 0.28 g per gram of host closely corresponds to the change in poros-

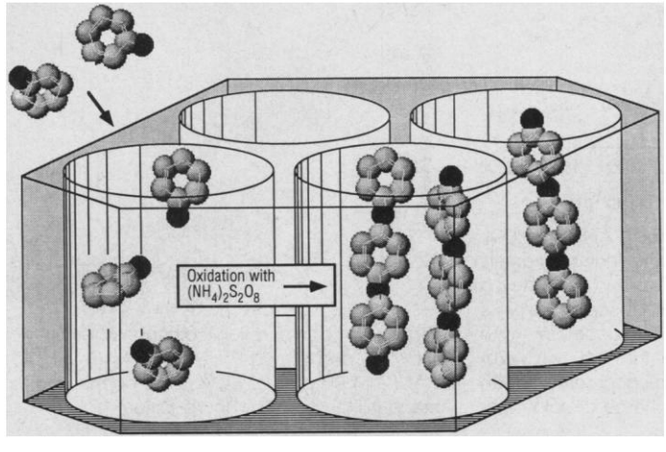


**Fig. 1.** Reaction scheme for the encapsulation of polyaniline in the channels of MCM-41.

Department of Chemistry, Purdue University, West Lafayette, IN 47907, USA.

*To whom correspondence should be addressed.

ity probed with nitrogen sorption. The general similarity of the unusual isotherm shapes suggests that a tubular structure is even maintained in the polyaniline-loaded host, but the shift of the saturation transition to lower partial pressure shows that the channels are now narrowed. The polymer morphology consistent with the sorption data is that of about a monolayer of PANI covering the walls of the MCM host. Given the structural data for model compounds of polyemeraldine salt (*23*), a geometric calculation shows that about 20 aligned polyaniline chains could fit in the 3-nm MCM channels if the latter were completely filled. Thermogravimetric analysis in oxygen (100 ml/min, heating at 5°C/min) indicates drastic changes in pyrolysis rate when the polymer is encapsulated. Whereas bulk emeraldine salt decomposes rapidly between 300° and 400°C, pyrolysis of the encapsulated polymer proceeds more slowly over a much greater temperature range (350° to 600°C). This difference indicates diffusional constraints in the channel system. The above results show that polyaniline was synthesized within the channels of the MCM host.

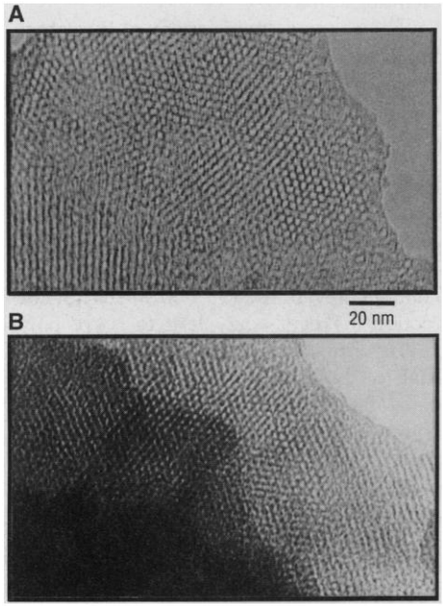


**Fig. 2.** Transmission electron micrographs of (**A**) MCM-41 and (**B**) PANI-MCM.

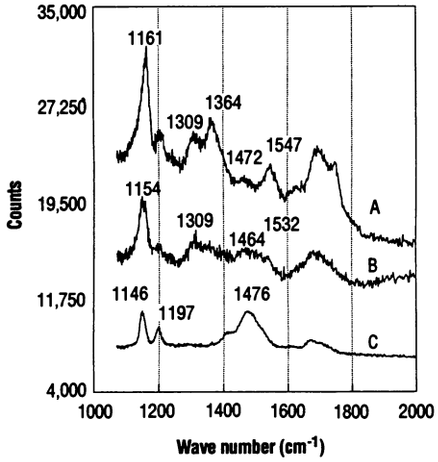


**Fig. 3.** Raman spectra of (curve A) PANI-MCM, (curve B) emeraldine salt, and (curve C) emeraldine base. The samples were irradiated with ~4 mW at 752 nm. Raman scattering was collected in backscattering geometry with *f*/0.95 optics and passed through two holographic filters into a 0.5-m monochromator with a liquid nitrogen–cooled charge-coupled device (CCD) detector.

Detailed studies of bulk emeraldine salt led to the model of a granular metal where charge hopping in amorphous regions between metallic bundles dominates the macroscopic conductivity (*24*, *25*). How does the polymer behave when it is encapsulated in nanometer channels? The dc conductivity of PANI-MCM is in the $10^{-8}$ S/cm range, similar to the conductivity of unloaded MCM host under ambient conditions and more than seven orders of magnitude lower than that for bulk PANI. When the polymer is extracted, the dc conductivity is $10^{-2}$ S/cm, a striking difference resulting from the removal of the separating MCM channel walls. This result confirms that the polyaniline is located inside the MCM channels and that no percolating conducting paths develop on the external crystal surfaces. To probe the charge transport of PANI filaments in the insulating MCM host, we used the contactless microwave absorption technique (*26*). The microwave conductivity of evacuated PANI-MCM (*27*) obtained from the perturbation of a rectangular cavity at 2.63 GHz is 0.0014 S/cm, one-fourth that of evacuated bulk PANI (0.0057 S/cm), after correction for the volume fraction of the polymer in the host. As synthesized, bulk polyaniline has a microwave conductivity of 0.018 S/cm and a dc conductivity of 0.2 S/cm. The significant low-field conductivity of the polymer filaments demonstrates that conjugated polymers can be encapsulated in nanometer channels and still support mobile charge carriers. In a previous study, we established that oxidized polypyrrole chains in the channels of zeolite Y and mordenite (0.7-nm channels) do not exhibit significant ac conductivity up to 1 GHz (*28*). The charge carriers are trapped in those systems, probably because of electrostatic interactions with the channel walls and the lack of interchain contacts. In contrast, the channels in the MCM host provide more space and allow some important interchain contact to occur.

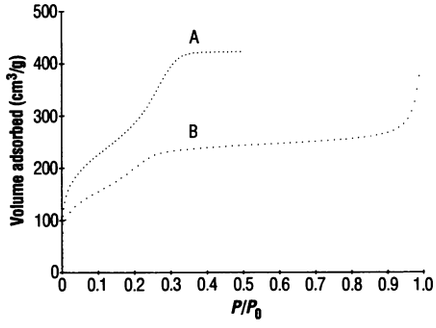


**Fig. 4.** Nitrogen sorption isotherms of (curve A) MCM-41 and (curve B) PANI-MCM (0.28 g of PANI in 1.00 g of host). Volume normalized to standard temperature and pressure (*P*); $P_o$ = 1 atm.

## REFERENCES AND NOTES


1. C. Carter, *Molecular Electronic Devices* (Dekker, New York, 1982).
2. A. Aviram, *J. Am. Chem. Soc.* 110, 5687 (1988); _____ and M. A. Ratner, *Chem. Phys. Lett.* **29**, 277 (1974).
3. A. Slama-Schwok, M. Blanchard-Desce, J. M. Lehn, *J. Phys. Chem.* **96**, 10559 (1992).
4. P. Seta *et al.*, *Nature* **316**, 653 (1985).
5. T. S. Arrhenius, D. M. Blanchard, M. Dvolaitzky, J. M. Lehn, J. Malthete, *Proc. Natl. Acad. Sci. U.S.A.* **83**, 5355 (1986).
6. R. Kopelman, S. J. Parus, J. Prasad, *Chem. Phys.* **128**, 209 (1988).
7. P. Enzel and T. Bein, *J. Phys. Chem.* **93**, 6270 (1989).
8. _____, *J. Chem. Soc. Chem. Commun.* **1989**, 1326 (1989).
9. T. Bein and P. Enzel, *Angew. Chem. Int. Ed. Engl.* **28**, 1692 (1989).
10. P. Enzel and T. Bein, *Chem. Mater.* **4**, 819 (1992).
11. C. R. Martin, R. Parthasarathy, V. Menon, *Synth. Met.* **55**, 1165 (1993), and references therein.
12. C. L. Curtis, J. E. Ritchie, M. J. Sailor, *Science* **262**, 2014 (1993).
13. J. S. Beck *et al.*, *J. Am. Chem. Soc.* **114**, 10834 (1992).
14. A. Monnier *et al.*, *Science* **261**, 1299 (1993).
15. W.-S. Huang, B. D. Humphrey, A. G. MacDiarmid, *J. Chem. Soc. Faraday Trans. 1* **82**, 2385 (1986).
16. A. G. MacDiarmid and A. J. Epstein, *Faraday Discuss. Chem. Soc.* **88**, 317 (1989).
17. S. P. Armes and J. F. Miller, *Synth. Met.* **22**, 385 (1988).
18. Raman spectra of polyaniline obtained with 632.8-nm excitation have been published [Y. Furukawa, T. Hara, Y. Hyodo, I. Harada, *ibid.* **16**, 189 (1986)]. The spectral positions observed here with excitation at 752 nm are shifted because of different resonance conditions. With excitation at 632.8 nm, a peak at ~1590 $cm^{-1}$ in the polyemeraldine base form was assigned to a *p*-substituted benzene ring vibration, which is shifted to ~1580 $cm^{-1}$ in the salt form. A peak at 1471 $cm^{-1}$ was associated with the mode of the unprotonated quinone dimine structure (mixed C=N and ring mode) that shifts to much lower energy on protonation (1344 or 1324 $cm^{-1}$), indicating a delocalized linkage between the rings. The latter vibrations can serve as markers for the protonated form. Another band of the resulting quinone radical cation structure was observed at 1484 $cm^{-1}$. Also, C–H in-plane bending occurs at about 1160 $cm^{-1}$.
19. Y. Furukawa *et al.*, *Macromolecules* **21**, 1297 (1988).
20. L. W. Shacklette, J. F. Wolf, S. Gould, R. H. Baughman, *J. Chem. Phys.* **88**, 3955 (1988).
21. H. H. S. Javadi *et al.*, *Synth. Met.* **29**, E439 (1989).
22. E. J. Oh *et al.*, *ibid.* **55–57**, 977 (1993).
23. The densities of crystalline model compounds of

polyaniline have been determined: phenyl-capped tetramer salt doped with 2 $BF_4^-$ and one acetonitrile per tetramer in the cell, 1.39 g/cm$^3$; phenyl-capped dimer, 1.25 g/cm$^3$ [R. H. Baughman, J. F. Wolf, H. Eckhardt, L. W. Shacklette, *Synth. Met.* **25**, 121 (1988)].
24. Z. H. Wang, E. M. Scherr, A. G. MacDiarmid, A. J. Epstein, *Phys. Rev. B* **45**, 4190 (1992).
25. H. H. S. Javadi, K. R. Cromack, A. G. MacDiarmid, A. J. Epstein, *ibid.* **39**, 3579 (1989).
26. D. C. Dube, M. T. Lanagan, J. H. Kim, S. J. Jang, *J. Appl. Phys.* **63**, 2466 (1988).
27. Evacuated at 25°C and $10^{-5}$ torr for 12 hours.
28. L. Zuppiroli, F. Beuneu, J. Mory, P. Enzel, T. Bein, *Synth. Met.* **55–57**, 5081 (1993).
29. We are grateful for partial funding from the Sprague Electric Company. The contribution of S. Esnouf to the ac conductivity measurements is greatly appreciated.

16 February 1994; accepted 22 April 1994

# Role of Deep Cloud Convection in the Ozone Budget of the Troposphere

Jos Lelieveld and Paul J. Crutzen

**Convective updrafts in thunderstorms prolong the lifetime of ozone ($O_3$) and its anthropogenic precursor $NO_x$ [nitric oxide (NO) + nitrogen dioxide ($NO_2$)] by carrying these gases rapidly upward from the boundary layer into a regime where the $O_3$ production efficiency is higher, chemical destruction is slower, and surface deposition is absent. On the other hand, the upper troposphere is relatively rich in $O_3$ and $NO_x$ from natural sources such as downward transport from the stratosphere and lightning; convective overturning conveys the $O_3$ and $NO_x$ toward the Earth's surface where these components are more efficiently removed from the atmosphere. Simulations with a three-dimensional global model suggest that the net result of these counteractive processes is a 20 percent overall reduction in total tropospheric $O_3$. However, the net atmospheric oxidation efficiency is enhanced by 10 to 20 percent.**

Deep cumulonimbus (Cb) convection is a primary mechanism for transporting heat, moisture, and momentum from the lower to the upper troposphere, thus forcing the general circulation of the atmosphere (*1*). In the Cb outflow region in the cold upper troposphere, cirrus clouds develop and cover areas much larger than the cores of these convective systems. The vigorous motions in the Cb cores, which tend to maximize in the mid-troposphere, are driven by the release of latent heat by condensation (*2*). Conversely, mesoscale descent in the cloud environment is caused by radiative and evaporative cooling and melting of ice (*3*). Upward transport through Cb clouds takes about 0.5 to 1 hour, whereas the mesoscale subsidence takes about 10 to 50 hours over a proportionally larger area (*4*). Although thunderstorms constitute a major force in the convective overturning of the troposphere, especially in the tropics, synoptic disturbances such as extratropical cyclones also cause rapid vertical mixing; vertical velocities in these systems are highest in the region of organized convection ahead of the frontal zone (*5*). Deep convective motions play an important role in the vertical redistribution of trace gases (*6*). In their absence, surface-emitted pollutants would be transported to the upper troposphere in several months, whereas through their presence large parts of the troposphere are mixed on much shorter time scales. In this study, a global three-dimensional transport–chemistry model of the troposphere was used to evaluate the effects of convection on the chemistry and distribution of $O_3$.

Ultraviolet radiation causes the photochemical formation of $O_3$; in the background troposphere this occurs mostly through the oxidation of carbon monoxide (CO) and methane ($CH_4$), catalyzed by $NO_x$ (*7*). The global budgets of these gases are dominated by anthropogenic emissions in the lower troposphere, notably from combustion (Table 1). In addition, in polluted or forested areas the oxidation of reactive hydrocarbons can play a significant role. In this study, we are concerned with the background troposphere; thus, we concentrate on the effects of CO and $CH_4$ oxidation. The lifetime of $NO_x$ in the troposphere is about 1 to 2 days, and that of CO is a few months. Hence, convection strongly alters the vertical profiles of these species, particularly that of $NO_x$. The photochemical $O_3$ yield per emitted $NO_x$ molecule decreases as $NO_x$ concentrations increase (*8*), so that the convective dilution of surface-emitted $NO_x$ from the boundary layer into the free troposphere enhances the formation of $O_3$. Moreover, the lifetime of $NO_x$ in the upper troposphere is longer by up to an order of magnitude than in the boundary layer. Chemical conversions and dry deposition act on $NO_2$ rather than NO. Ultraviolet radiation fluxes and thus photolysis rates are relatively high and temperatures are low in the upper troposphere, which shifts the equilibrium between $NO_2$ and NO toward NO. Also, in the absence of deposition processes nitric acid ($HNO_3$) accumulates so that $NO_x$ can partly reform through photodissociation and reaction with hydroxyl (OH). Furthermore, the lifetime of $O_3$ that has been formed photochemically in the boundary layer is enhanced by upward convective transport. At low altitudes, $O_3$ is efficiently destroyed by deposition on land surfaces (*9*) and through $O_3$ photolysis and subsequent reaction of $O(^1D)$ with water vapor; the latter reaction, yielding OH, is most efficient in the humid lower troposphere. Consequently, it has been concluded that convective transport of $O_3$ and its surface-emitted precursors enhances the tropospheric $O_3$ abundance (*6*, *10*). We show, however, that this assessment may not be true.

In the classical theory regarding tropospheric $O_3$, downward transport from the stratosphere is the dominant $O_3$ source (*11*). Although there is no agreement about the relative contributions of downward $O_3$ mixing and in situ photochemical $O_3$ formation, several studies suggest that the anthropogenic release of $O_3$ precursors is of major importance in the contemporary tro-

**Table 1.** Model trace-gas emissions (in teragrams per year) (*16*), of which two-thirds are from anthropogenic sources in the lower troposphere.

| Source | CO | $CH_4$ | $NO_x$ |
|---|---|---|---|
| Fossil fuel use | 450 | 115* | 25 |
| Biomass burning | 400 | 30 | 9 |
| Natural | 470† | 135‡ | 11.5§ |
| NMHC oxidation | 230‖ | | |
| Ruminants | | 105¶ | |
| Rice paddies | | 70 | |
| Landfills | | 40 | |
| Sewage | | 25 | |
| Total | 1550 | 520 | 45.5 |

*Includes 5 Tg/year from $CH_4$ hydrate destabilization. †Three hundred teragrams per year from natural nonmethane hydrocarbon (NMHC) oxidation in the atmosphere, 100 Tg/year from vegetations, 40 Tg/year from oceans, and 30 Tg/year from wildfires. ‡Thirty teragrams per year from high-latitude wetlands and 70 Tg/year from low-latitude wetlands, 20 Tg/year from termites, 10 Tg/year from oceans, and 5 Tg/year from wild ruminants. §Five teragrams of N per year from lightning, 6 Tg of N per year from soils, 0.5 Tg from the stratosphere. ‖From anthropogenic NMHC oxidation in the atmosphere. ¶Includes 25 Tg/year from animal wastes.

J. Lelieveld, Wageningen University, Air Quality Department, Post Office, Box 8129, 6700 EV Wageningen, Netherlands.
P. J. Crutzen, Max-Planck-Institute for Chemistry, Atmospheric Chemistry Division, Post Office Box 3060, 55020 Mainz, Germany and the Center for Clouds, Chemistry, and Climate, University of California, San Diego, CA 93093-0221, USA.